

Compression After Impact on Honeycomb Core Sandwich Panels with Thin Facesheets, Part 1: Experiments

Thomas D. McQuigg¹ and Rakesh K. Kapania²
Virginia Polytechnic Institute and State University, Blacksburg, VA, 24060

Stephen J. Scotti³ and Sandra P. Walker⁴
NASA Langley Research Center, Hampton, VA, 23681

A two part research study has been completed on the topic of compression after impact (CAI) of thin facesheet honeycomb core sandwich panels. The research has focused on both experiments and analysis in an effort to establish and validate a new understanding of the damage tolerance of these materials. Part one, the subject of the current paper, is focused on the experimental testing. Of interest are sandwich panels, with aerospace applications, which consist of very thin, woven S2-fiberglass (with MTM45-1 epoxy) facesheets adhered to a Nomex honeycomb core. Two sets of specimens, which were identical with the exception of the density of the honeycomb core, were tested. Static indentation and low velocity impact using a drop tower are used to study damage formation in these materials. A series of highly instrumented CAI tests was then completed. New techniques used to observe CAI response and failure include high speed video photography, as well as digital image correlation (DIC) for full-field deformation measurement. Two CAI failure modes, indentation propagation, and crack propagation, were observed. From the results, it can be concluded that the CAI failure mode of these panels depends solely on the honeycomb core density.

¹ Graduate Research Assistant, Aerospace and Ocean Engineering, 215 Randolph Hall, Student Member AIAA

² Mitchell Professor, Aerospace and Ocean Engineering, 215 Randolph Hall, Associate Fellow AIAA

³ Structures and Materials Chief Engineer, Research Directorate, Mail Stop 162, Member AIAA

⁴ Supervisory Research Aerospace Engineer, Structural Mechanics and Concepts Branch, Mail Stop 190, Member AIAA

I. Introduction

Vehicles today are increasingly built from composite structures, such as honeycomb core sandwich panels, which often feature thin, laminated facesheets. Structures such as these are highly susceptible to large residual strength reductions due to damage which may not be readily apparent. This damage can come from a wide variety of sources, one of which is low velocity impact. The compression response of thin facesheet sandwich panels to loading after being subjected to low velocity impact damage is the focus of the present research. A comprehensive review on the subject of damage tolerance in sandwich construction composite materials was written by Tomblin, Lacy, Smith *et al.* [1] and published by the Federal Aviation Administration (FAA). The authors discussed sources of localized damage resulting from low to medium velocity impacts include damage during manufacturing, assembly, and handling (e.g. tool drops) and in-service operation (e.g. hail or bird strikes).

The incentive for the FAA to establish a document on damage tolerance in composites was to ascertain an approach for future designs to meet government safety requirements for airframe certification. The report by Tomblin, Lacy, Smith *et al.* [1] describes two critical standards which were considered in the present research. First, the authors established relationships between representative damage sizes to design load requirements. The smallest level of damage is defined below the Allowable Damage Limit (ADL) threshold. This, sometimes undetectable, damage is also known as Barely Visible Impact Damage (BVID), a common term in the study of composite impact damage. An airframe is required to withstand this type of damage over the operational lifetime of the vehicles without repair at no decrease in ultimate failure load capability. A second damage level, where the damage is viewable but may not be found except by periodic inspection, is defined below the Critical Damage Threshold (CDT). Aircraft are required to be able to withstand damage up to CDT while undergoing multiple loadings between specified inspection intervals and at least one lifetime limit load. Damage beyond the CDT is defined as readily apparent to the operator of the vehicle (such as bird strike or engine burst). (This approach was later formally adopted as guidance for development

and certification of composite structures by the FAA [2].)

In a second critical standard recommended in the report by Tomblin, Lacy, Smith *et al.* [1], a five step methodology for describing composite airframe damage tolerance is explained. First, damage formation in a specific sandwich structure subject to low-velocity impact must be investigated experimentally. In the second step, sandwich panel coupons are tested for residual strength (e.g. CAI testing). In the third task, damaged sandwich panels are subjected to fatigue loading, which is important in characterizing types of damage up to the CDT. In step four, a model for predicting impact damage development and residual strength degradation should be developed. The fifth and final state of the recommended methodology for determining damage tolerance is component, and then full-scale testing and verification of the model results.

In the present document, the first of a two-part research initiative on the damage tolerance of two sandwich composite material systems is described. The experimental testing presented here closely aligns with steps one and two of the five-step methodology described above. For the two material systems, a set of damage formation tests, and a set of CAI tests completed on each material system will be described. In a second, subsequent report, an analysis model will be described which aligns with step four of Ref [1]. The experimental results will be used to validate this model. First, a brief review of the literature currently available on the subject of experimental CAI testing of sandwich structures will be given. This brief review will discuss damage formation in and CAI testing of sandwich composites, including key techniques, damage and failure characteristics. An expanded review can be found in the Ph.D. Dissertation by McQuigg [3].

A. Damage Formation by Low Velocity Impact

In the present research, damage formation is studied using both low-velocity impact testing using a drop tower, and static indentation. A typical impact tower was used in the research by Raju, Smith, Tomblin *et al.* [4], which consisted of an impactor apparatus of a given mass, with a given tip size and shape, dropped from a height appropriate to the impact energy level of interest. The authors have shown that each of these parameters affects the size, shape, and types of damage present after an impact. Typical testing using static indentation was described by Singh, Davidson,

Eisenberg *et al.* [5]. Static indentation produces similar damage to low velocity impact and is easily repeatable. However, static indentation results will be shown to be conservative for damage formation in a material.

Impact damage in a composite sandwich structure can be present in both the facesheets and the core. In the present research, the facesheet materials are laminated woven fiberglass with epoxy resin. Cantwell and Morton [6] identified several failure mechanisms due to impact in fiber reinforced polymer (FRP) composite laminates, including fiber-matrix debonding, fiber pull-out, intralaminar matrix cracking, matrix deformation, delamination, and fiber fracture. The failure mechanisms described are applicable to both unidirectional and woven fabric FRP laminates, and to composite sandwich facesheets which are made from these materials. Tomblin, Lacy, Smith *et al.* [1] also mentioned several types of impact damage unique to sandwich composites, facesheet-core delamination, core crush, and puncture.

Raju, Smith, Tomblin *et al.* [4] also identified a series of damage progression for increasing impact energy in composite sandwich structures. The first type of damage they identified for the lowest levels of impact energy is the initiation of facesheet and core damage. This includes the onset of core crush and plastic deformation of the facesheet which may be accompanied by local constituent damage and failure. Second, the damage propagates through the facesheet (by subsequent constituent or bonding failure) and the core (by crushing). In the third stage, the facesheet may fracture for some sandwich constructions, especially with thick core, while the core may just consolidate for thinner cores. Extreme damage becomes apparent in the fourth stage as complete facesheet penetration occurs and the core completely consolidates. Finally, in the fifth and most extreme stage of impact damage for a material, damage is initiated in the backside facesheet.

B. Compression After Impact Testing

A good overview of the CAI test procedure was given by Tomblin, Raju, Liew *et al.* [7]. In general, CAI testing involves the placement of an impact damaged material coupon in a compressive end-loaded condition. Clamped conditions are simulated at the load application ends of the specimen, and some fixtures may stabilize the panel from buckling by simulating simply supported

conditions along the non-load application sides. Typically, the impact damage is located in the center of the test coupon, and strain gages are placed to each side of the damaged location as well as on the undamaged facesheet in the case of sandwich constructions. Multiple strain gages may be used if a strain distribution is desired. Also, force resultant is usually recorded, as well as applied displacement information. CAI residual strength results are usually presented as a function of impact energy, but can also be presented versus other damage measures such as planar damage or maximum indentation.

Rhodes [8] [9] studied impact and CAI failure in composite sandwich panels at NASA Langley Research Center several decades ago. First, specimens were surveyed to determine the impact velocities and corresponding energies of interest. Rhodes found that the areas of delamination in sandwich panels were much smaller than laminate plates impacted similarly. However, areas of crippled honeycomb core were present beneath the impact areas. Rhodes observed only a sharp well defined facesheet crack as the resulting failure mode of compression testing these specimens. The facesheets of Rhodes' panels were very thick.

More recently, an example of an experimental study by Raju, Smith, Tomblin *et al.* [4] studied the CAI strength in honeycomb core sandwich panels with both glass fiber reinforced polymer (GFRP) and carbon FRP facesheets with damage at various impact energy levels from two different size indentors. Three failure mechanisms were observed, which are common to several other CAI studies. First, some panels failed by strength failure across the width initiating at the damage location. Second, some panels failed by indentation propagation mechanism, and finally in a third class of failure the indentation propagation is started but then is arrested and facesheet strength failure follows for the remaining width of the specimen.

Tsang and Lagace [10] conducted an interesting experimental study on composite sandwiches to separate the influences of core damage and facesheet damage and thus determine each factor's effect on the compressive failure mode of the sandwich. They showed that core damage had to be present to instigate the dimple propagation failure mode seen in this and other experimental studies, but the presence of facesheet damage accelerated this failure mode. They also showed that facesheet layup determined the final shape of the resulting facesheet crack propagation.

C. Overview of Part 1 of the Research

The present report describes Part 1 of a body of research consisting of experiments and analysis on the CAI response of thin facesheet honeycomb core sandwich panels. This first part pertains to the experimental work which has been completed. The current section has introduced the research topic and briefly described some highlights of the literature review which was completed. The remainder of Part 1 of the research will discuss the damage resistance and damage tolerance of two sets of composite sandwich structures, which are described in the following section. A damage formation study, consisting of static indentation and impact using a drop tower apparatus, will be described. The results of the damage formation study were then used to select the impact energy levels of interest for CAI testing. These levels are primarily correspond to BVID, as well as higher levels of damage. A set of CAI experiments was then completed on 24 CAI test coupons, while using a variety of instrumentation to capture the response of each test coupon during compressive loading and at coupon failure. Failure modes are observed using high speed photography, and digital image correlation techniques and equipment. Results are shown for both damage formation and CAI tests. Unique insight on the influence of the honeycomb core density on the sandwich panel's response is provided.

II. Materials and Test Coupons

Damage formation and CAI tests were performed on two series of materials fabricated specifically for this research initiative by AAR Composites, using aerospace grade materials. Both material systems were fabricated with woven, GFRP facesheets and Nomex hexagonal cell honeycomb core. The designation given to each of the two material systems was based on the density of the honeycomb core included in each sandwich construction. 3PCF-XX series coupons contain a core with 3 lb/ft³ (PCF) density and 6PCF-XX series coupons contain a core with 6 lb/ft³ (PCF) density. All other material properties are shared by the two material systems. Both cores are 0.75 in. thick and have a 0.125 in. nominal cell size.

The facesheets of both the 3PCF-XX and the 6PCF-XX material systems consisted of two plies, each of style 6781 woven S2-glass fabric cloth with 35% MTM45-1 epoxy resin content. The

facesheets of these two sandwich panel systems were very thin gage as they consisted of two plies, and the nominal facesheet thickness was 0.02 in. The facesheet plies of these new material systems were oriented with ply directions of 0° and 45° . The overall sandwich panel was a symmetric $[0/45/\text{CORE}/45/0]$ construction for both material systems. The 3PCF-XX and 6PCF-XX sandwich materials are shown in Fig. 1. The core gives the 3PCF-XX material a yellow hue through the translucent facesheets, while the 6PCF-XX series panels are green for the same reason. The translucent property also allows for improved visual inspection for damage that may be present in the material.

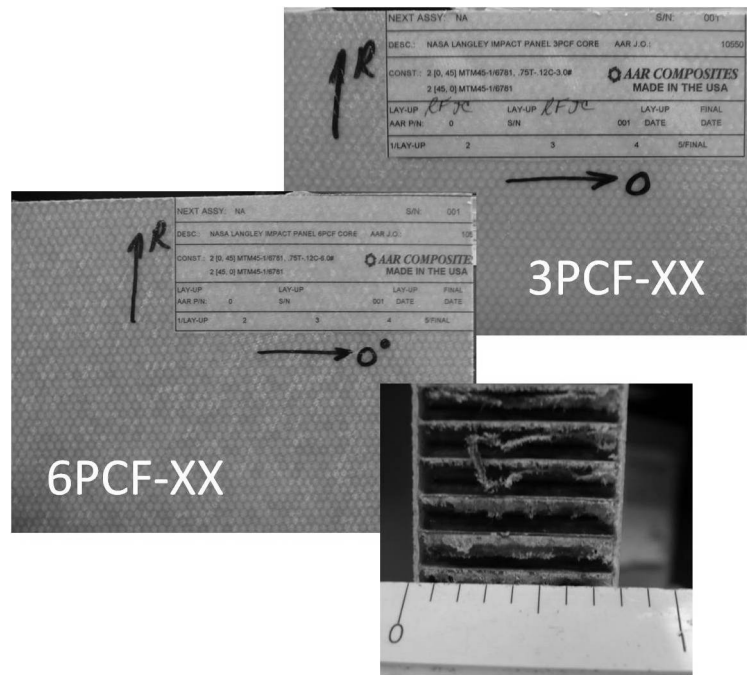


Fig. 1 3PCF-XX (top) and 6PCF-XX (middle) series honeycomb core sandwich panels, and side view (bottom).

The facesheet material has the following properties, as measured by the National Institute for Aviation Research[11]. The warp (0°) direction strength and moduli are listed as 81.46 ksi and 4.22 Msi, respectively, for tensile loading, and 83.43 ksi and 4.22 Msi, respectively, for compressive loading. The fill (90°) direction strength and moduli are listed as 80.50 ksi and 4.07 Msi, respectively, for compressive loading, and 69.07 ksi and 4.02 Msi, respectively, for tensile loading. The in-plane shear strength and modulus are 5.45 ksi and 0.550 Msi, respectively. The in-plane Poisson's ratio

is 0.138.

The Nomex honeycomb core properties for the 3PCF-XX material systems are listed as tested on a 0.5 inch thick specimen. The out-of-plane strength and modulus is 270 psi and 20 ksi, respectively. The shear strengths are listed as 140 psi for the L direction (ribbon direction) and 74 psi for the W direction. The shear moduli are listed as 4.5 and 2.5 ksi for the L and W directions, respectively. For the 6PCF-XX material system, the higher density Nomex honeycomb core properties are as follows from tests on samples of 0.5 in. thickness. The out-of-plane crush strength and modulus are 925 psi and 60 ksi, respectively. The shear strengths are 330 psi and 170 psi for the L and W directions, respectively. The shear moduli are 13.0 and 6.5 for the L and W directions, respectively. The experimental test data presented here, for the honeycomb core materials used, is available from HexCel Composites, Inc. [12].

Test coupons for damage formation and CAI testing of 3PCF-XX and 6PCF-XX materials were fabricated at the nominal size of 5.5 in. by 5.5 in. This size was chosen based on recommendations of ASTM test standards [13] [14], as well as to maximize the available source material. Examples of the test coupons are shown in Fig. 2. The load introduction ends of CAI test coupons were “potted” to limit erroneous failure mechanisms using a unique method developed during this research. A section of core material was removed from between the facesheets on each of these coupons. This section had dimensions of the width (6 in.) and thickness (0.75 in.) of the coupon and extended in the loading direction approximately 0.5 in. A piece of wood was cut to tight tolerances and set in place of the removed core material with an epoxy resin. The wood limits the contraction of the potting material while it cures, which improves load transfer to the CAI test coupon. The load application ends of each coupon was ground to straight and level to a tolerance of 0.001 in.

III. Impact Damage Formation

Two types of tests were used to characterize damage formation in these two materials for a range of energy levels: static indentation and impact testing using a drop tower. In addition, the results of these tests were then used to select the impact energy levels of interest for CAI testing. The energy levels of interest for the 3PCF-XX and 6PCF-XX series materials were representative of low velocity

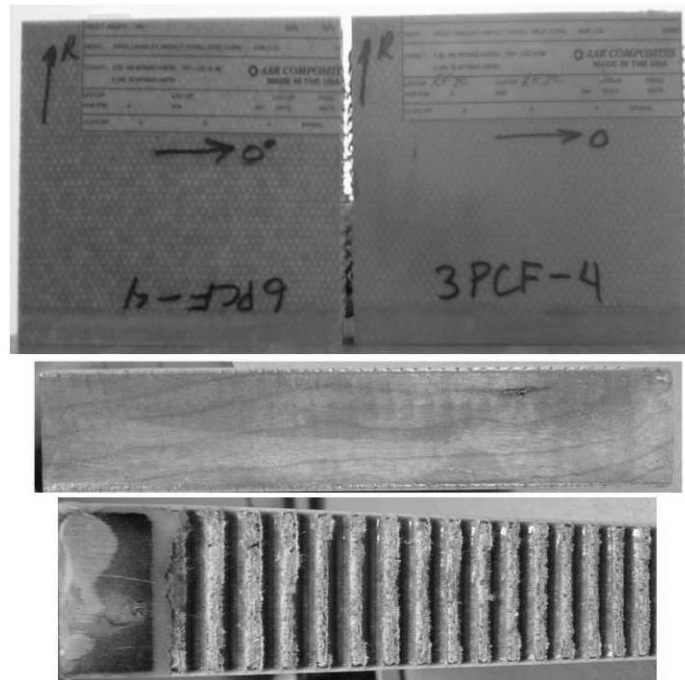


Fig. 2 3PCF-XX (top right) and 6PCF-XX (top left) series material coupons for testing, with top load bearing end (middle) and side views (bottom).

impacts which would cause low to moderate damage to the impacted sandwich panel. The highest levels of damage included complete facesheet penetration and core crushing through greater than 50% of the coupons thickness. The range of damage included barely visible impact damage (BVID) and extended to clearly visible damage. The testing procedures, apparatus, instrumentation, and results for static indentation and drop impact on 3PCF-XX and 6PCF-XX series materials will be described in the following sections.

A. Static Indentation

Static indentation is a controlled, easily repeatable method of causing damage in composite sandwich panels. In this research, it was used to gain an initial understanding of the types of damage which would appear in the panels for various energy levels. Although the types of damage from static indentation are similar to impact damage, this method produces more damage for a given energy level than a low velocity impact. Based on the results of this research, static indentation is considered by the authors to be a conservative method of estimating impact damage resistance in a

given material. A hydraulic testing machine was used for static indentation using a 0.5 in. diameter hemispherical tip. Static indentation of 3PCF-XX and 6PCF-XX series sandwich coupons is shown in Fig. 3.

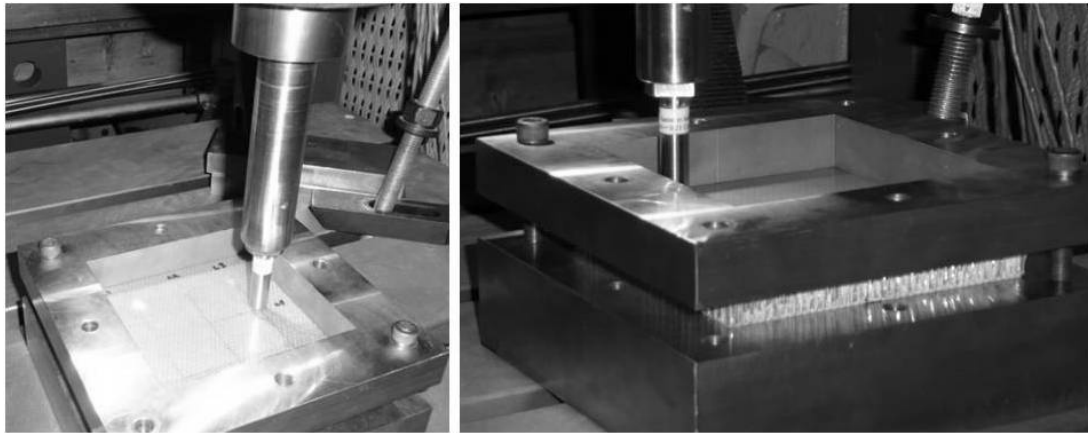


Fig. 3 Static indentation of 3PCF-XX (right) and 6PCF-XX (left) series sandwich coupons.

Indentations of 3PCF-XX and 6PCF-XX series materials were conducted while the coupons were clamped on all four edges using a metallic frame which allowed for the coupon to be suspended with the rear, undamaged facesheet unsupported. The test frame used to prescribe these conditions to the static indentation coupon and can be seen in Fig. 3. One coupon of each material was used for static indentation and several indentations were made in each coupon at various locations. The quasi-static loading was displacement controlled and applied at a rate of 0.05 inch per minute. The applied displacement and the reaction force were recorded for each indentation.

Five static indentations were made into a 3PCF-XX material coupon to investigate the coupon's response. The results of static indentation are shown in photographs in Fig. 4. The static indentation test at *Location 1* on the coupon was used to find the resultant force measured at facesheet fracture. Facesheet fracture occurred at 171 lbs and 0.133 in of applied displacement. By integration of the reaction force vs. applied displacement results, the energy absorbed was found to be 0.914 ft-lb. Visible facesheet damage included inter-fiber fracture (IFF, i.e. matrix cracking) in a circular region centered at the point of indentation. For larger indentations, fiber fracture was also present. Fiber and matrix fracture appear randomly oriented and saturate the area of damage.

The force vs. displacement results for all five static indentation tests can be seen in Fig. 5.

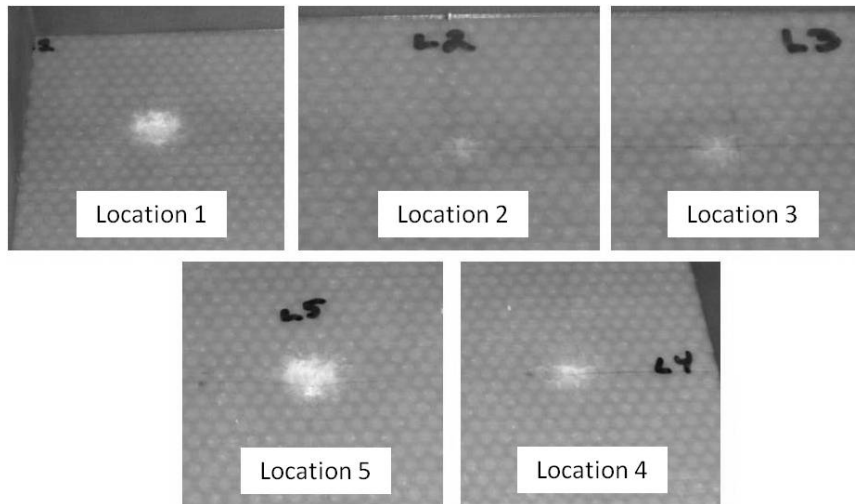


Fig. 4 Results of static indentation of 3PCF-XX series material coupons: residual dents.

Facesheet fracture occurred in tests at *Location 1* and *Location 5* and can be seen as a sudden drop in resultant force while the applied displacement is still being increased. Tests were also conducted to 50, 100, and 150 lbs. nominally, for *Locations 2, 3, and 4*, respectively.

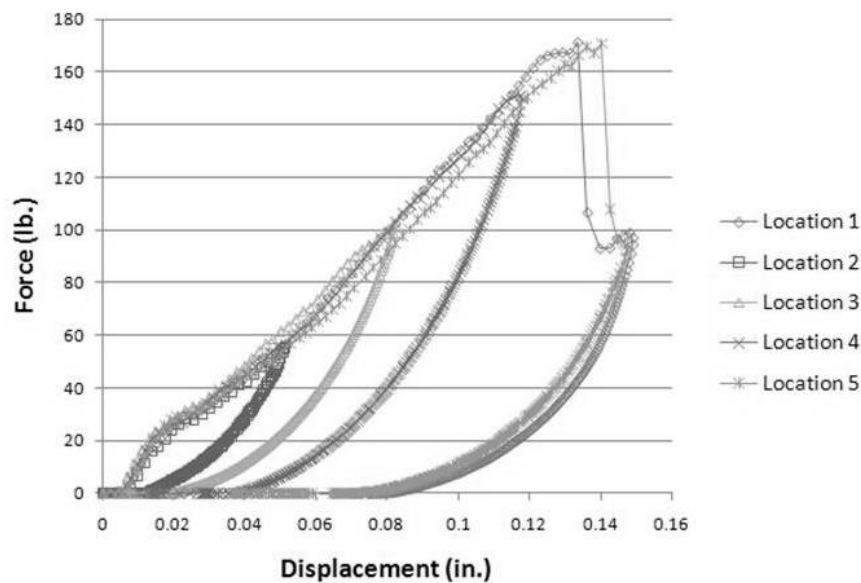


Fig. 5 Results of static indentation of 3PCF-XX series material coupons: resultant force vs. applied displacement.

Six static indentation tests were then completed on a 6PCF-XX series material coupon. The resulting dents and damage can be seen in Fig. 6. Force vs. displacement results for these inden-

tation tests are shown in Fig. 7. The first indentation was again used to determine the load and energy required for facesheet fracture. Failure occurred at 205.1 lbs. and 0.101 in. of indentation. By integration, the energy absorbed was found to be 0.891 ft-lb. The resulting damage found in this material is similar to damage in 3PCF-XX materials, at similar energy levels. In addition to indentations made to facesheet failure at *Locations 1* and *5*, indentations were made to 50, 100, 150 and 180 lbs. at *Locations 2, 3, 6, and 4*, respectively. More static indentation results can be found for both 3PCF-XX and 6PCF-XX materials in the Ph.D. Dissertation by McQuigg [3].

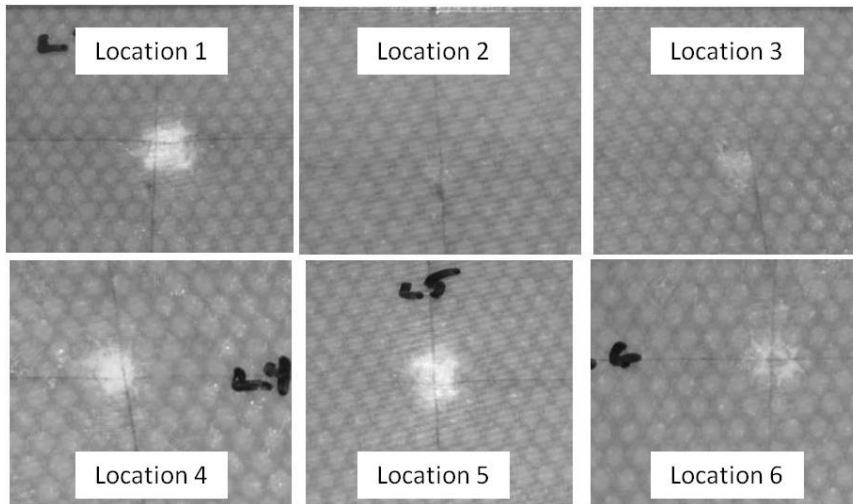


Fig. 6 Results of static indentation of 6PCF-XX series material coupons: residual dents.

B. Drop Tower Impact Survey

An impact damage survey of 3PCF-XX and 6PCF-XX materials was completed using a drop tower. The purpose of the impact survey was to determine the characteristic damage at various impact energy levels and to make a decision about which energy levels to study during CAI tests. For the impact survey tests, a material coupon was clamped on all four edges with no support under the opposite facesheet, to simulate a realistic impact. The test fixture was then clamped beneath the drop tower apparatus, as shown in Fig. 8.

The drop tower consisted of a metal tube several yards in length, mounted vertically. An electronic pulley system was mounted to the tube to raise the impactor and to set the drop height. Once in place the impactor was dropped with the press of a button, which activated a mechanical

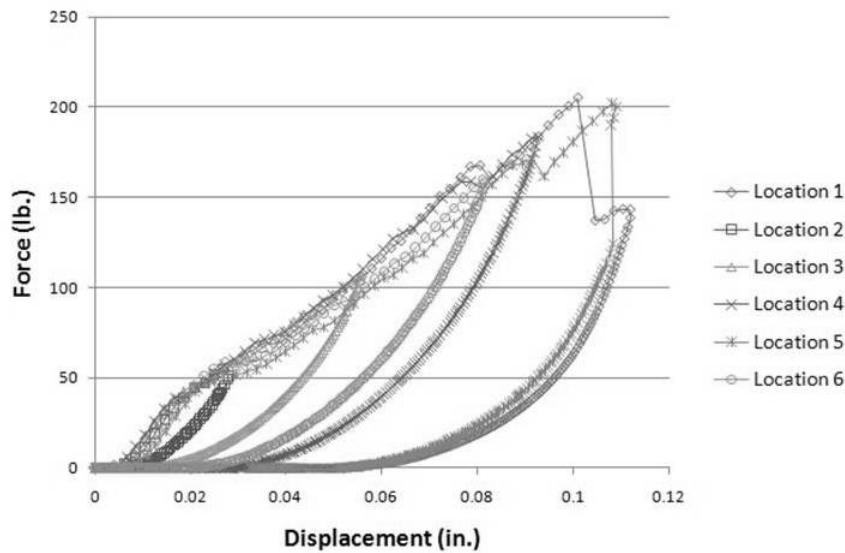


Fig. 7 Results of static indentation of 6PCF-XX series material coupons: resultant force vs. applied displacement.

release. Upon impact the mass would rebound from the coupon and a mechanical catch would spring into place automatically to catch the impactor before it could strike the coupon a second time. Impacts were conducted with a 0.5 in. hemispherical tip and the weight of the impactor with the tip attached was measured to be 2.4855 lb. The drop height could be set using the impact tower apparatus to the nearest tenth of an inch.

Once an impact on a 3PCF-XX or 6PCF-XX series material coupon was conducted, the residual dent was measured in terms of its maximum depth and diameter. After the coupons were visually examined, they were later carefully dissected with through-thickness cuts through the center of each of the indentations in order to assess the condition of the honeycomb core beneath the indentation. Maximum thickness and width of the crushed core region (measured from the bottom of the dented facesheet) was measured using inspection by optical microscopy. In addition to this information, the impact force was recorded electronically with respect to time so that the *impact length* could also be determined. The impact length is the time in seconds from when the impactor comes into contact with the sandwich panel specimen, to when it rebounds completely. In addition, measured and visual qualitative observations were made about the location and characteristics of other types of damage present, including cracking or penetration of the impacted facesheet. Results versus

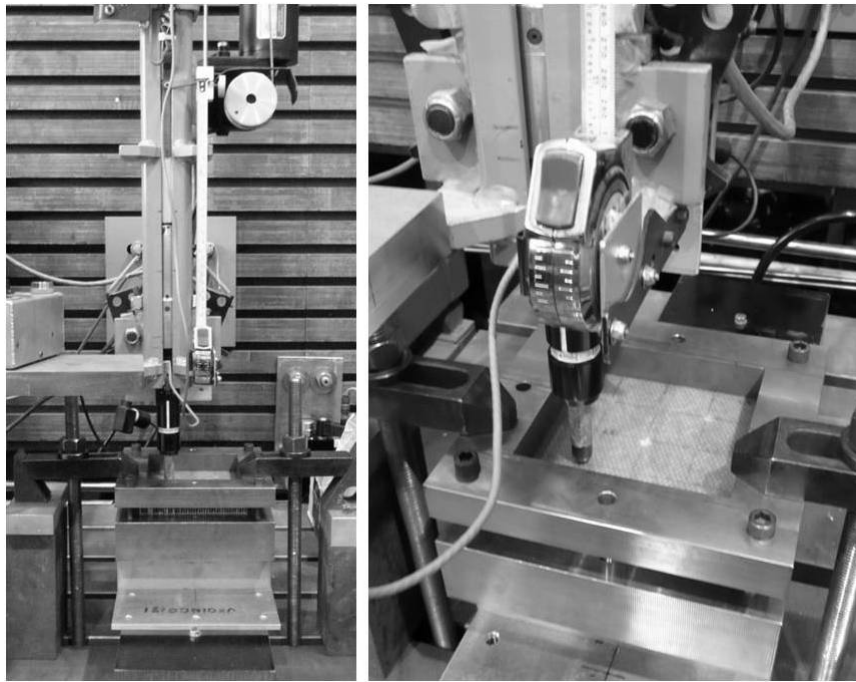


Fig. 8 Drop tower apparatus used for impact survey of 3PCF-XX and 6PCF-XX series material coupons.

impact energy for residual dent depth, residual dent diameter, maximum impact force, and impact length are shown in Figs. 9, 10, 11, and 12, respectively. Results for comparisons of crushed core diameter (width), crushed core depth, and total damage depth comparisons for both 3PCF-XX and 6PCF-XX materials are shown in Figs. 13, 14, 15, and 16, respectively. Further impact survey results can also be found in Ref. [3].

Impacts on 3PCF-XX and 6PCF-XX materials with energies ranging from 1 to 9 ft-lb. were surveyed. The higher energies became of interest because this type of damage had not been considered for CAI strength prediction in thin facesheet sandwich panels. For the 3PCF-XX material, when impacted at 8 ft-lb. the impactor completely impacted the first facesheet and became lodged in the sandwich panel. Since this was well beyond the damage levels of major impact, 9 ft-lb. was not considered. 3.5 ft-lb. was considered instead for the ninth impact location on the specimen. Facesheet fracture occurred at 4 ft-lb. for both types of panels. This can be seen in Fig. 9 where the dent depth suddenly becomes much larger with increasing impact energy. The maximum impact force also increases with impact energy until impact levels at which facesheet fracture occurs, and

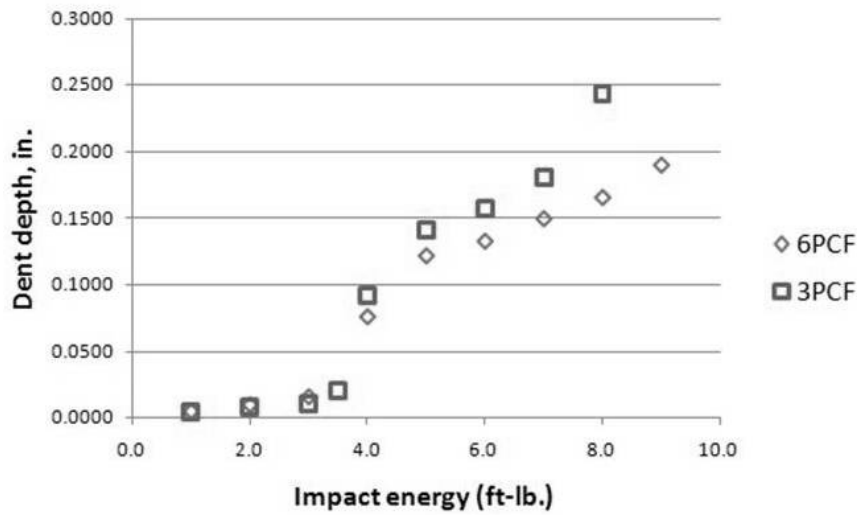


Fig. 9 Results of drop tower impact testing on 3PCF-XX and 6PCF-XX series materials: variation of the dent depth vs. the impact energy.

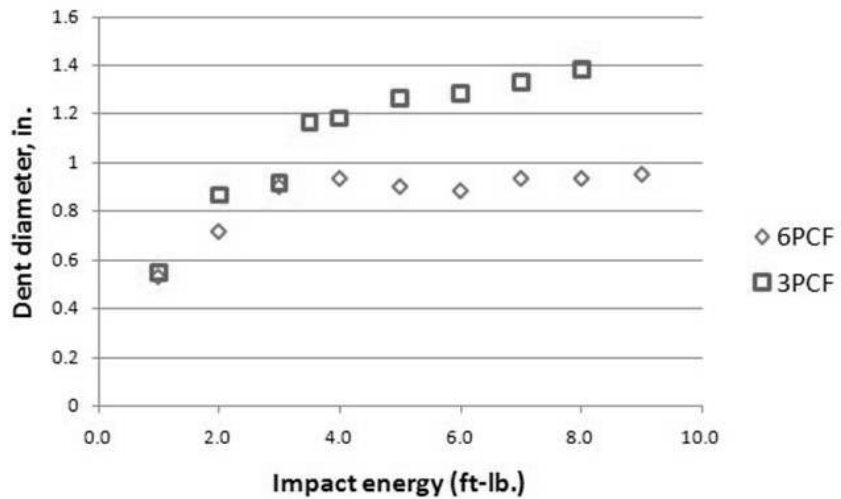


Fig. 10 Results of drop tower impact testing on 3PCF-XX and 6PCF-XX series materials: variation of the dent diameter vs. the impact energy.

then reaches a maximum. Impact length is longer for impacts where fracture occurred due to the decreased rebound speed as more energy is absorbed by the panel, contributing to damage. Core damage was considered in detail for 3PCF-XX and 6PCF-XX panels. Figure 13 shows that the width of the damaged core region is higher for 3PCF-XX panels than for 6PCF-XX, in general. Also, the maximum thickness of the crushed core region is higher for damage regions in 3PCF-XX materials. The conclusion can be made from these results that the higher strength and stiffness of

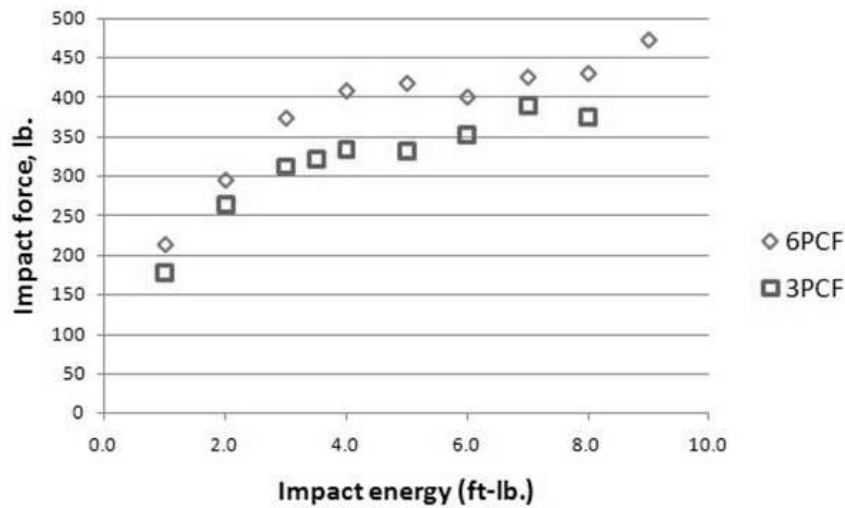


Fig. 11 Results of drop tower impact testing on 3PCF-XX and 6PCF-XX series materials: variation of the maximum impact force vs. the impact energy.

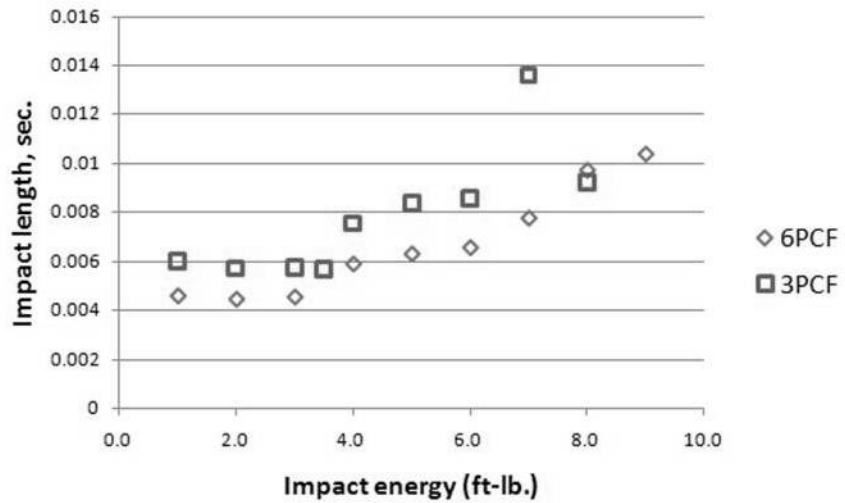


Fig. 12 Results of drop tower impact testing on 3PCF-XX and 6PCF-XX series materials: variation of the impact length vs. the impact energy.

the 6PCF-XX material's core has a significant effect on the impact resistance of the sandwich panel. It is also interesting to note that the depth of the core crush region beneath the indented facesheet stays about the same for all levels of impact energy.

Several types of damage are present in the impact locations on the 3PCF-XX series materials shown in Fig. 17, and the 6PCF-XX materials shown in Fig. 18. At very low impact energy levels, 1 to 3 ft-lb. for 3PCF-XX, and 1 to 2 ft-lb. for 6PCF-XX, there is a slight discoloration of the

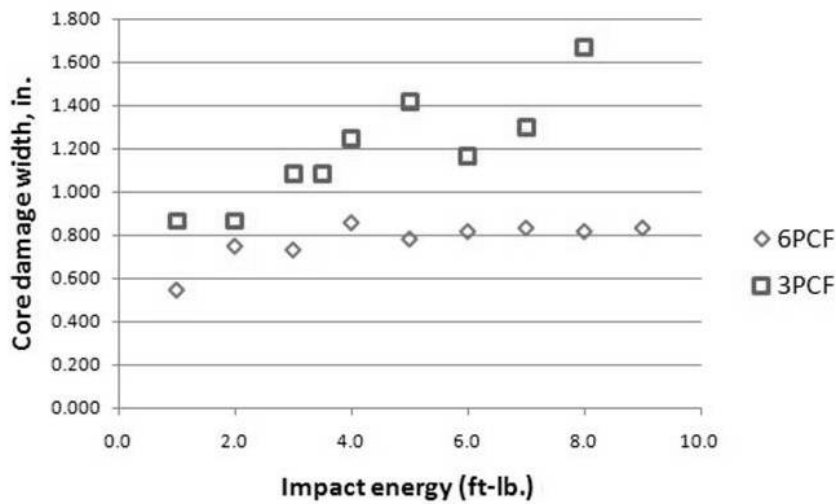


Fig. 13 Results of drop tower impact testing on 3PCF-XX and 6PCF-XX series materials: variation of the core damage width vs. the impact energy.

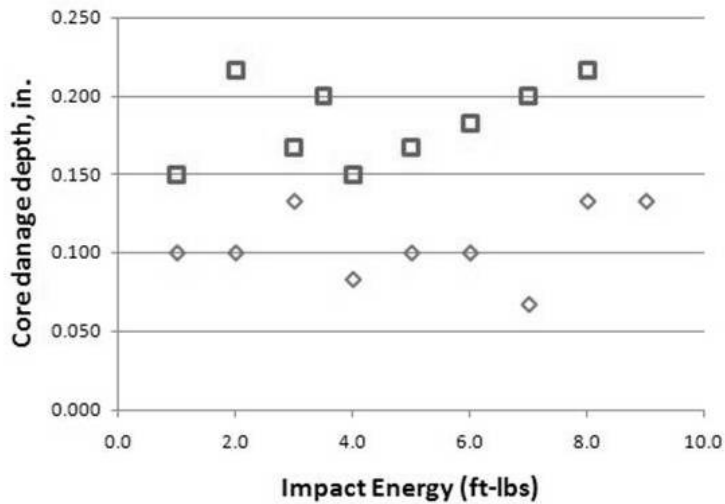


Fig. 14 Results of drop tower impact testing on 3PCF-XX and 6PCF-XX series materials: variation of the core damage depth vs. the impact energy.

facesheet and almost imperceptible residual dents in the facesheet, which are shown graphically in Figs. 9 and 10. These levels are considered barely visible impact damage (BVID) as they would be difficult to find even during routine inspection, especially if the facesheets were coated with paint. The maximum impact energy level associated with BVID is about 3 ft-lb. for both sets of materials; although, for the less stiff 3PCF-XX materials it may extend marginally higher. At higher energy levels, the facesheet fracture is very noticeable. At levels of 6 ft-lb. and higher, there is practically

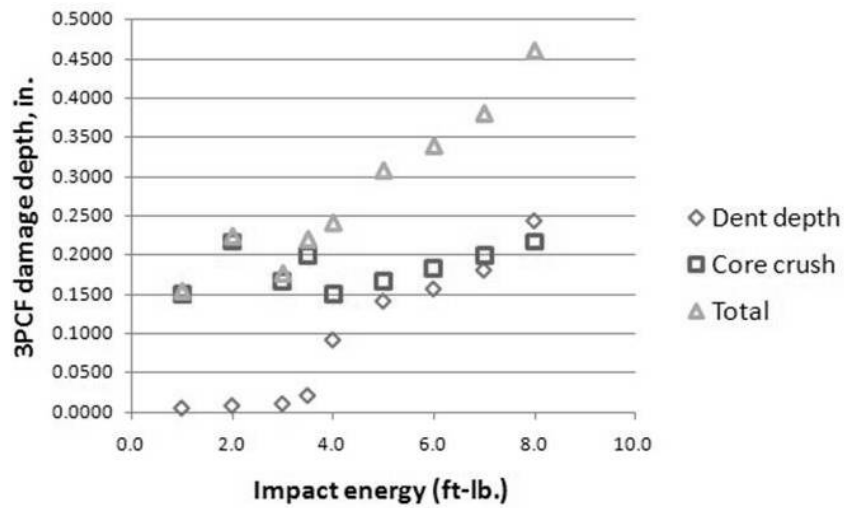


Fig. 15 Results of drop tower impact testing on 3PCF-XX and 6PCF-XX series materials: variation of the total dent depth for 3PCF-XX materials vs. the impact energy.

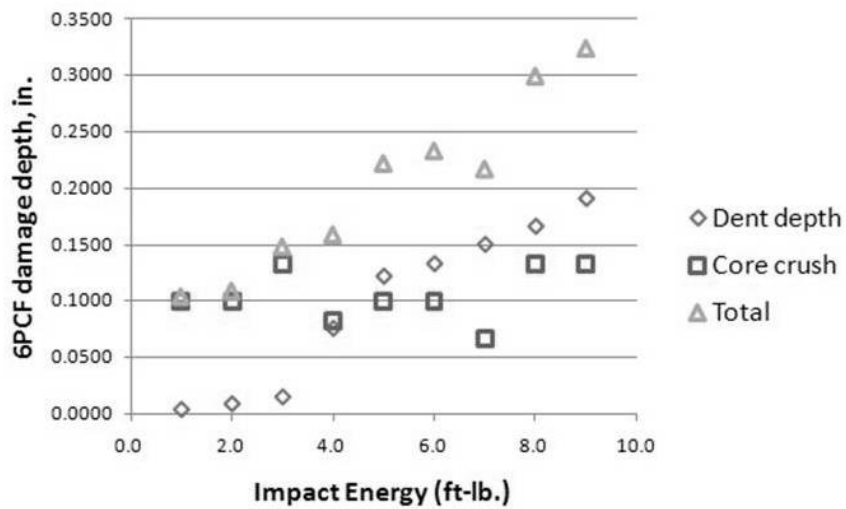


Fig. 16 Results of drop tower impact testing on 3PCF-XX and 6PCF-XX series materials: variation of the total dent depth for 6PCF-XX materials vs. the impact energy.

an open hole in the facesheet. Photographs of damage cross sections, taken after cuts were made, show that significant core damage is also present for panels with this amount of facesheet damage. An example of these cross-sections is shown in Fig. 19. At higher energy levels, the core damage present includes large amounts of tearing and bears little resemblance to the hexagonal cellular structure.

The data collected, as a result of the impact survey of 3PCF-XX and 6PCF-XX series sandwich

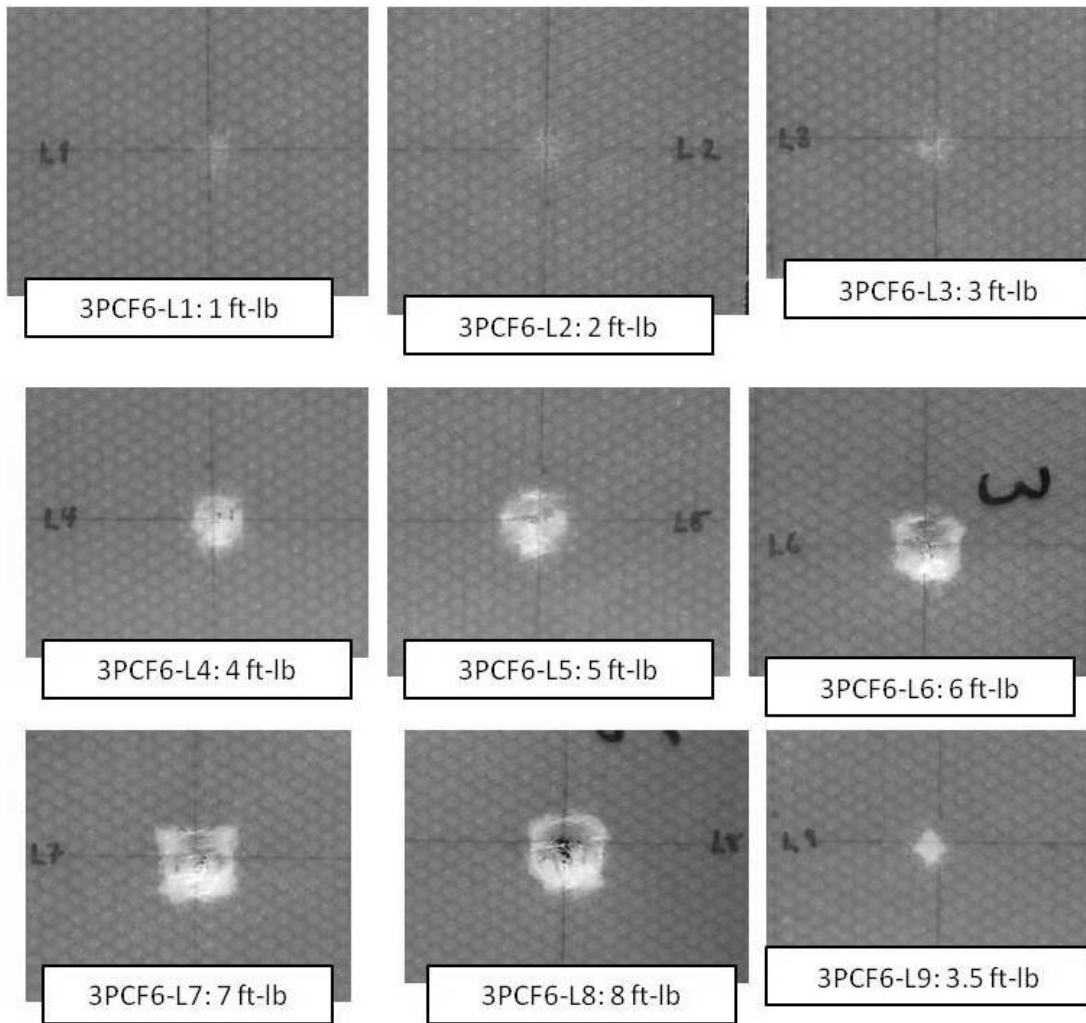


Fig. 17 Results of drop tower impact testing on 3PCF-XX series materials: residual dents.

panels, helped establish the energy levels of interest for various CAI test coupons. During the impact survey, impact energy levels of 1 to 9 ft-lbs. were considered for both sets of materials. Impact energy levels of 1, 3, 5, and 7 ft-lb. were chosen for impacts on CAI test coupons. Undamaged coupons would also be tested to find the sandwich construction's undamaged compressive strength.

IV. Compression After Impact

Several test methods were considered when the CAI tests described in this section were designed. ASTM standard test methods (STM) were consulted, but an ASTM STM for CAI of sandwich constructions has not currently been adopted. The ASTM STM for compressive residual strength of composite plates does describe a procedure and special test fixture for simple plates with centrally

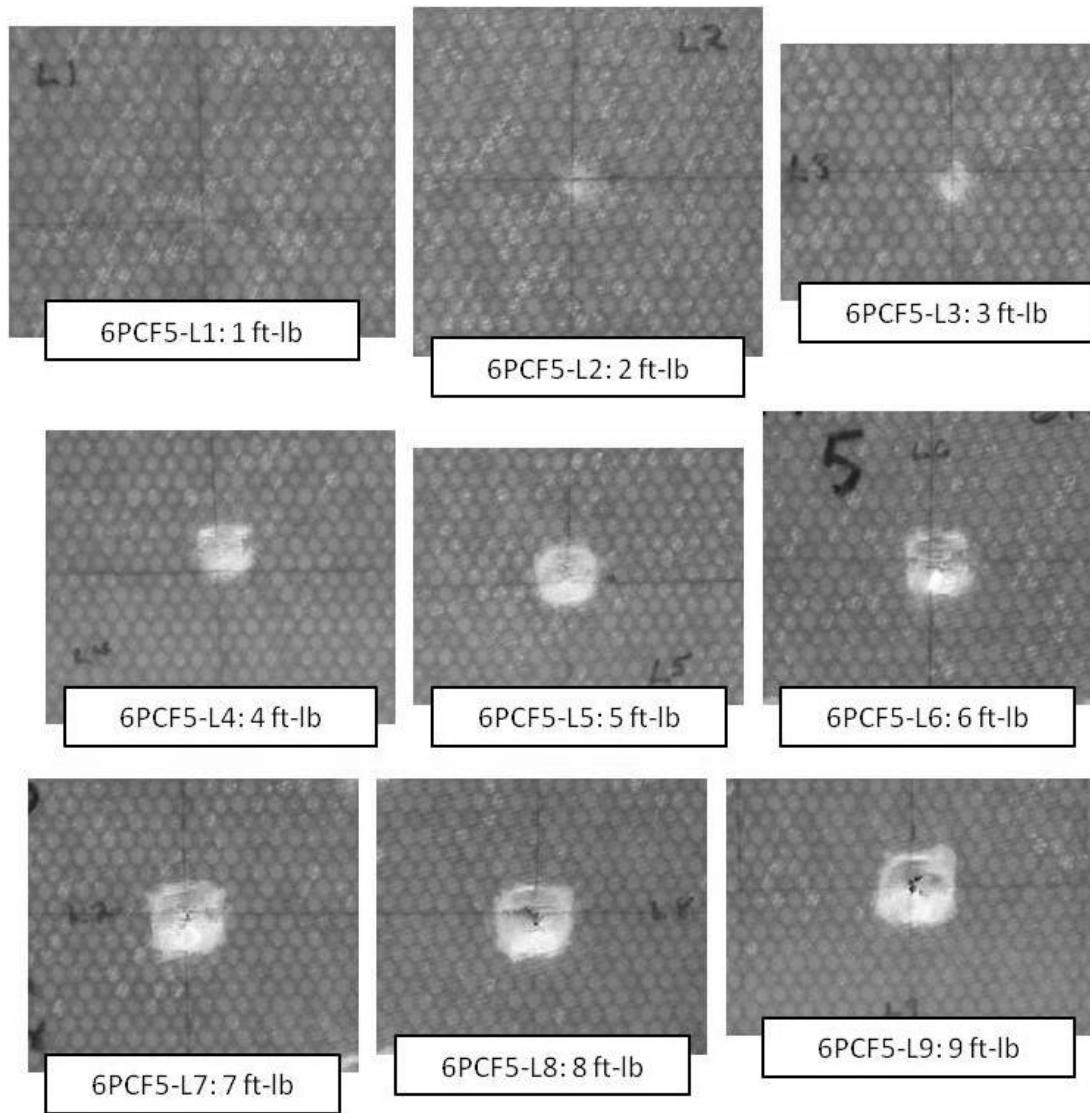


Fig. 18 Results of drop tower impact testing on 6PCF-XX series materials: residual dents.

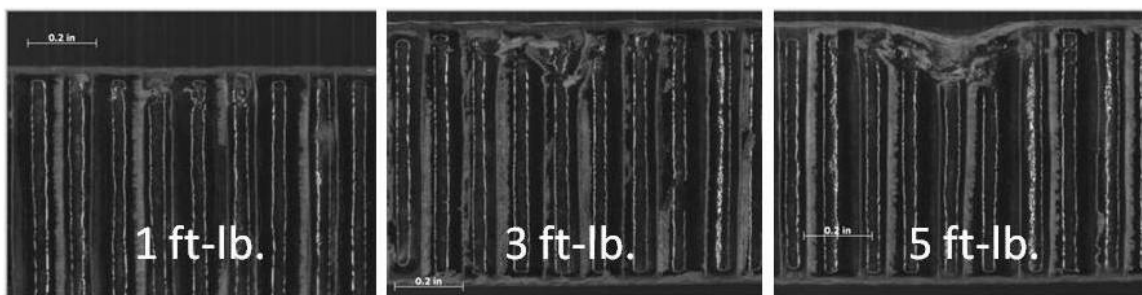


Fig. 19 Results of drop tower impact testing on 6PCF-XX series materials: core damage shown through destructive evaluation.

located impact damage [13]. This reference was consulted for strain gage placement and allowable

failure modes. The ASTM STM for edge-wise compressive strength (undamaged) of sandwich constructions was also considered [14]. This test method was consulted for sizing of the damaged panels, since the increased bending stiffness of sandwich constructions should preclude the use of the test fixture described in Ref. [13]. The next sections of this report will describe the apparatus and the instrumentation used for CAI testing, and present the results obtained.

A. Apparatus and Instrumentation

Compression after impact coupons of 3PCF-XX and 6PCF-XX series materials were mounted in a servo-hydraulically actuated MTS load frame. The test coupons were clamped at the top and bottom, placed on top of an adjustable bearing, and mounted on the MTS load frame between its two square loading platens. On the load frame, the top platen remained fixed, while the lower platform was also adjustable. The adjustable bearing and lower platen could be used to adjust the position of the sandwich panel coupon with a small load applied to facilitate a uniform compressive loading condition, free from significant bending moments. Compressive loading was displacement controlled and applied at a rate of 0.01 in. per minute. The load frame with a 3PCF-XX series coupon installed and a close-up picture of a 6PCF-XX coupon installed within the apparatus are shown in Fig. 20.

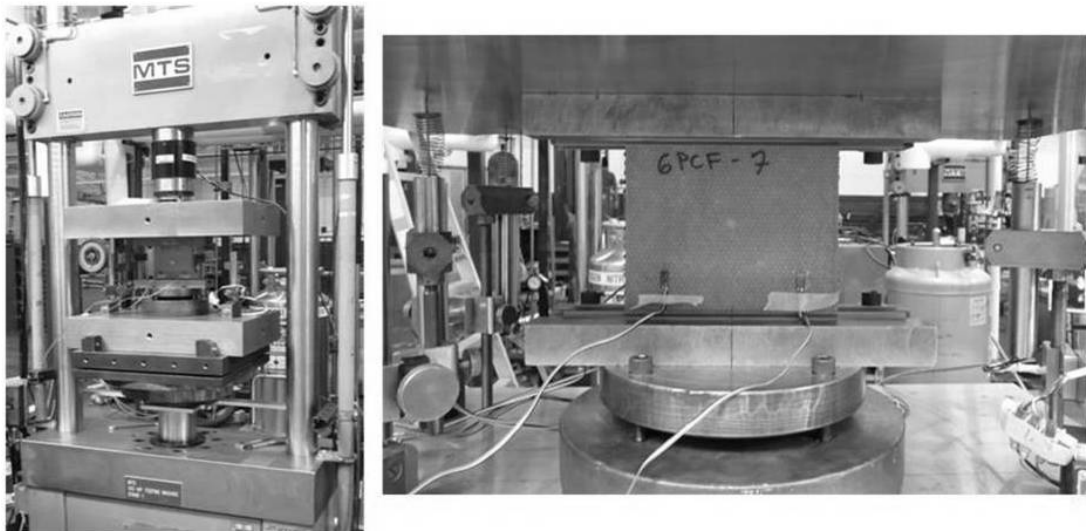


Fig. 20 Load frame and coupon mounting apparatus used for CAI testing with 3PCF-XX (left) and 6PCF-XX (right) coupons installed.

For all CAI test, the applied displacement and the measured reaction force were recorded. Far field strain in the direction of loading was recorded on the front and rear facesheets of each CAI coupon throughout testing. In general, four uniaxial strain gages were placed on the specimen as shown in Fig. 21. At least three of the strain gages numbered 1 through 4 in Fig. 21 were necessary to assure coupon alignment within the loading apparatus. For select panels, a biaxial strain gage was used in place of uniaxial gage #3 in order to facilitate measurement of Poisson's effects in the coupon. Three direct current displacement transducers (DCDT) were mounted to monitor the displacement at several locations between the loading platens. A fourth DCDT was used to measure the out-of-plane displacement of the center of the rear (undamaged) facesheet.

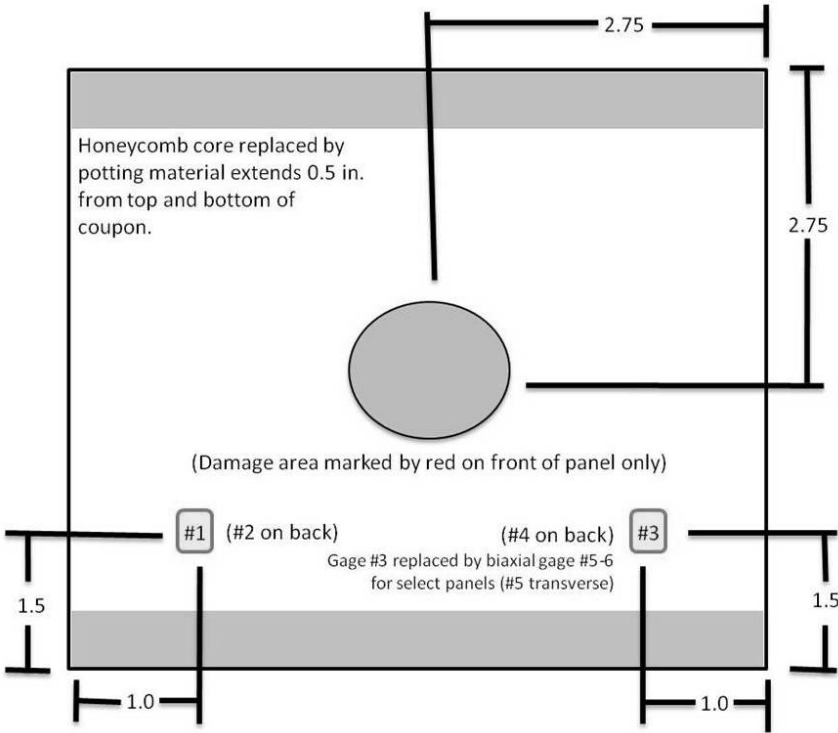


Fig. 21 Location of strain gages for CAI testing (all dimensions in inches).

Several types of auxiliary instrumentation were used throughout CAI testing. Real time video imagery was taken of select CAI tests using a handheld digital camera. Ambient temperature and humidity were noted for each specimen. In addition, high speed footage using a Phantom camera system [15] was used for select panels. Two Phantom cameras were used for high speed video photography of CAI failure. One was placed in front of the test frame, while a second camera was

placed at an angle to one side in order to capture the out of plane displacement seen during some CAI failures. On further selected test specimens, digital images for digital image correlation (DIC) measurements of full-field, three dimensional displacement and strain were taken using a VIC-3D system [16].

The DIC system allows for collection of full three-dimensional (3D) displacements associated with the region of interest during testing. This is done by measuring the change in location of a series of unique points (or “speckles”) located on the specimen in the field of interest. The VIC-3D software then can be used to calculate strains for the region of interest. For the purpose of this testing, the entire front, damaged facesheet, visible between the clamps at the top and bottom of the coupon, was the field of interest. The mounted strain gages must be removed from the field of interest due to optical distortion. In preparation for measurements by DIC, the entire front facesheet is spray-painted white after the strain gages have been mounted. Afterwards, speckles are added based on the size of the field of view, the displacements expected, and the digital cameras. Two digital cameras are used to capture two synchronous images from which the software can recognize and correlate each unique speckle in 3D space. Once the system is in place and calibrated, displacement measurements can be made using each image pair and information obtained through calibration, such as camera location with respect to target, and various optical image distortion parameters. More information can be obtained on image correlation theory in the resource by Sutton, Orteu, and Schreier [17].

At least one panel damaged at each impact energy level, for each material system, was considered by each auxiliary instrumentations (i.e. coupons damaged at 1 ft-lb. were observed with both high speed photography, real time photography, and DIC, just not at the same time).

B. CAI Test Results

Twenty-four coupons were centrally impacted on one facesheet of each specimen. Impacts at energy levels of 1.0, 3.0, 5.0, and 7.0 ft-lb. were carried out on three coupons each, for both 3PCF-XX and 6PCF-XX materials. Damage was inflicted using the 0.5 in. diameter hemispherical shaped tip. Information about the resulting damage, as well as the test specimen identifiers, impact energy,

and the resulting failure loads are shown in the Appendix of Ref. [3]. A displacement controlled compressive load was applied to each coupon until failure occurred, marked by a sudden drop in the measured reaction force, as shown in Fig. 22. The region with no data points at the beginning of the test is due to the CAI test data recording beginning with some load applied. The reason for this is some load (around 1500 lb.) is applied during specimen alignment, and this was only reduced to 1000 lb. before the beginning of the test.

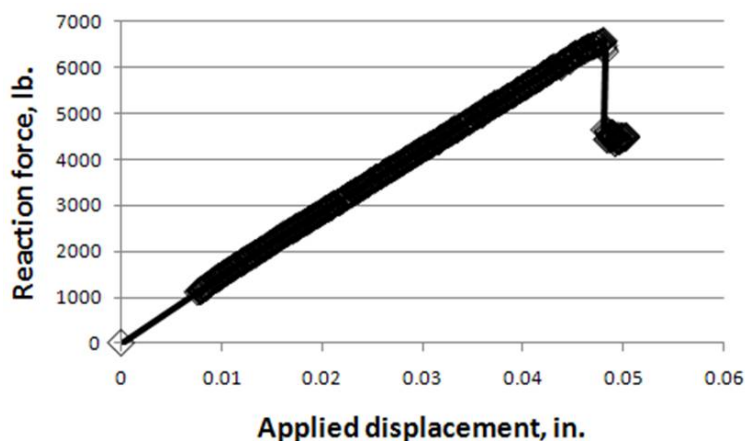


Fig. 22 Sample force vs. displacement results for a CAI test.

In addition, two undamaged coupons (one of each material type) were tested to failure to establish the initial compressive strength of the coupons. The compressive strength result for 3PCF-14 was the higher of the two panels tested and is considered more accurate since failure occurred at the clamped end for 6PCF-8. It is expected that the two types of panels should have nearly identical undamaged compressive strengths since the facesheet constructions are the same, and undamaged compressive failure should be controlled by facesheet strength.

Global failure of each 3PCF-XX and 6PCF-XX CAI coupon occurred because of failure in the damaged facesheet only. The rear facesheet still carried some load prior to failure. Two failure modes were seen during CAI testing. The failure mode of the 3PCF-XX panels was indentation propagation. The failed 3PCF-XX specimens have a region of local buckling, extending transverse to the direction of applied load, from the residual dent initially imposed by the low velocity impact. The 6PCF-XX panels failed by a second, different failure mode. Instead of a region of local buckling, only a crack appears in the initially damaged facesheet, although it propagates similarly to the

indentation propagation. The differences between the two failure modes can clearly be seen in Fig. 23, which shows two test coupons, post-failure, while still loaded.

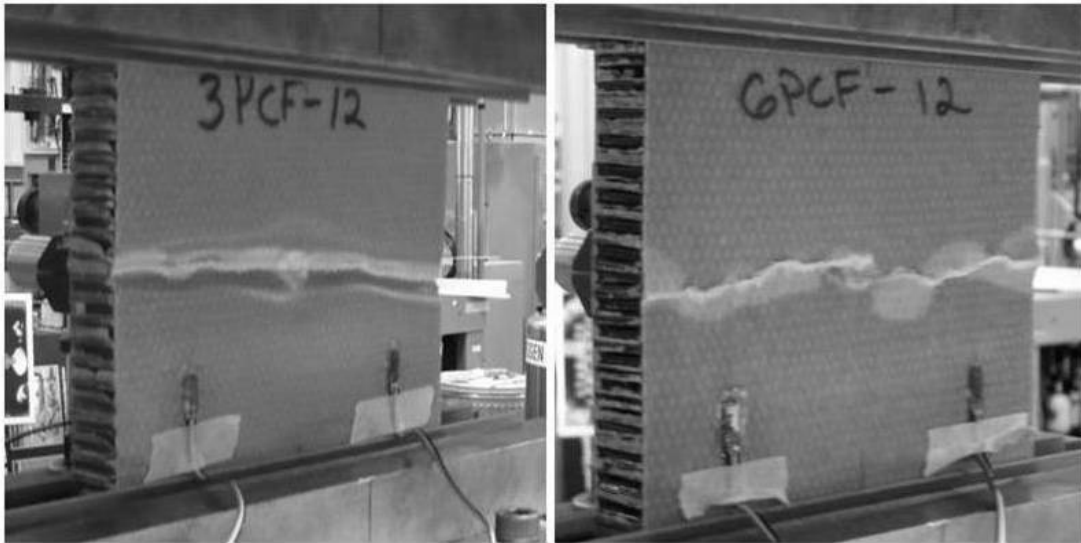


Fig. 23 Failure modes of indentation propagation for 3PCF-XX series coupons (left) and crack propagation in 6PCF-XX coupons (right).

Video photography was also used for select tests of 3PCF-XX and 6PCF-XX materials. Time lapse photography of a 3PCF-XX series coupons shown in Fig. 24 indicates several interesting features of an indentation propagation failure. This example is for a specimen impacted with at a 7.0 ft-lb. impact energy level, but the results are similar for all the 3PCF-XX series test coupons. The stable indentation growth is apparent beginning at just over halfway through the test, shown at the 1 minute, 33 second mark in Fig. 24. A crack also propagates in a stable fashion once the indentation is large enough. In less damaged test specimens, the crack propagates with the indentation growth. At failure the crack and the indentation can be seen to grow transversely to the applied load.

Time lapse photography of a 6PCF-XX series coupons shown in Fig. 25 indicates that the initial dent grows very little prior to the specimen failure. It appears to be nearly the same size at 1000 lbs. of load as it does at 5000 lbs. of load for coupon 6PCF-3. This particular coupon was impacted at 5 ft-lbs. of energy, but this was typical of all 6PCF-XX series CAI tests. At about the 4 minute mark, a small crack in the front facesheet appeared, advancing from the initial damage location transverse

to the load direction (vertical). By the 4 minute, 30 second mark, the crack had advanced slightly; however, by the 5 minute mark the crack was easily visible and the panel was very near to the residual strength which was found to be 6107 lbs. for the 6PCF-2 coupon. Between the 5 minute, 3 second and the 5 minute, 4 second marks in the real time video, the crack propagated to the edge of the specimen (accompanied by some interlaminar delamination and facesheet debonding), thus compromising the facesheet.

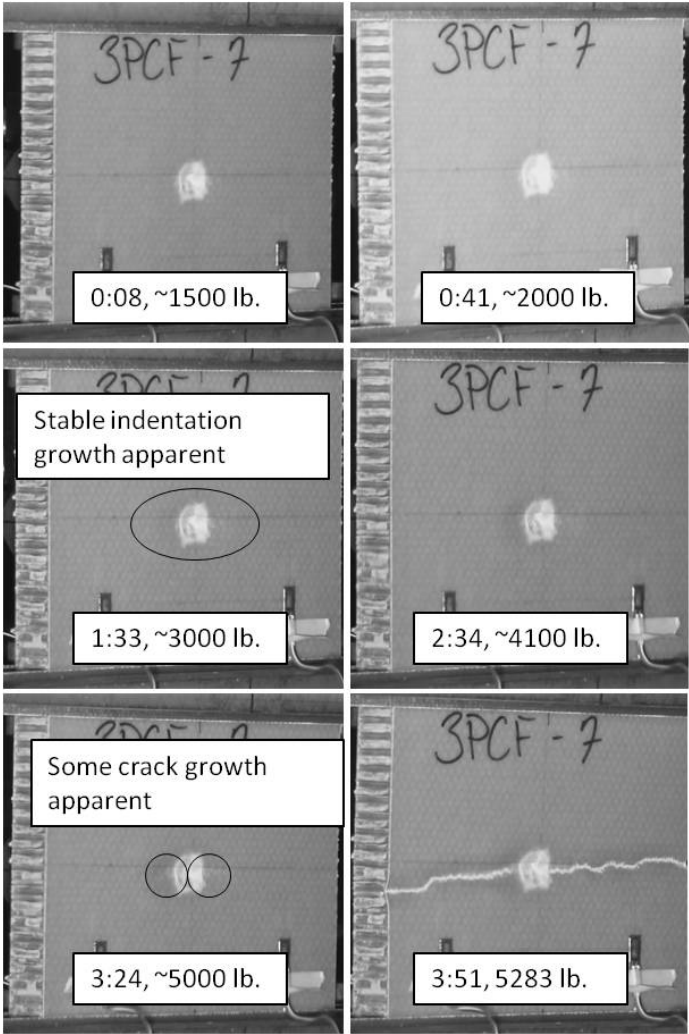


Fig. 24 Time lapse images of 3PCF-XX CAI test.

The high speed camera systems used to capture failure of both 3PCF-XX and 6PCF-XX series materials were quite essential in fully understanding failure, as it happens rapidly in real time. A Phantom version 12 [15] video system captured front views of select panels at 15,001 photos per second and a Phantom version 7 [15] video system captured side angles at 12,500 photos per second

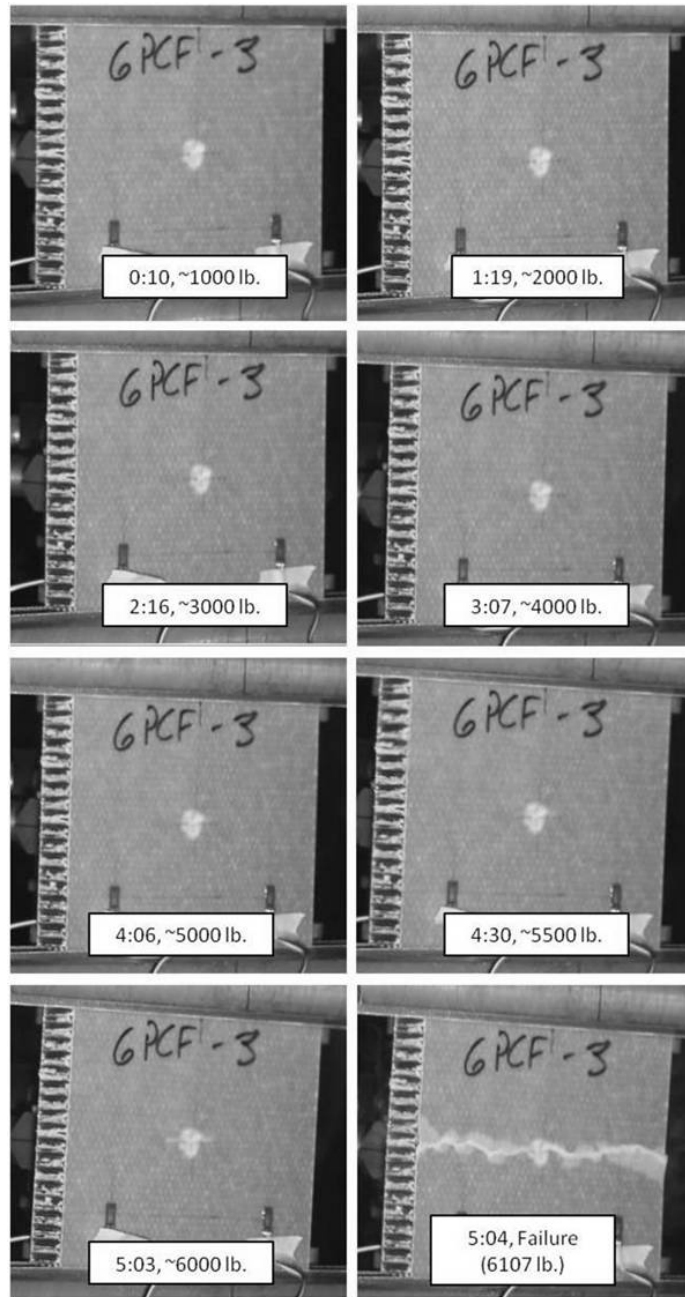


Fig. 25 Time lapse images of 6PCF-XX CAI test.

to illustrate any out-of-plane displacement of the facesheets. Frames taken from footage captured from both view points during CAI testing of coupons 6PCF-12 and 3PCF-15 show, in Fig. 26, the contrasting failure modes occurring during the moment of failure.

The sequences taken from the two cameras for 6PCF-12 begin with a small crack already visible growing from the initial impact initiated indentation. The crack propagates quickly to each side,

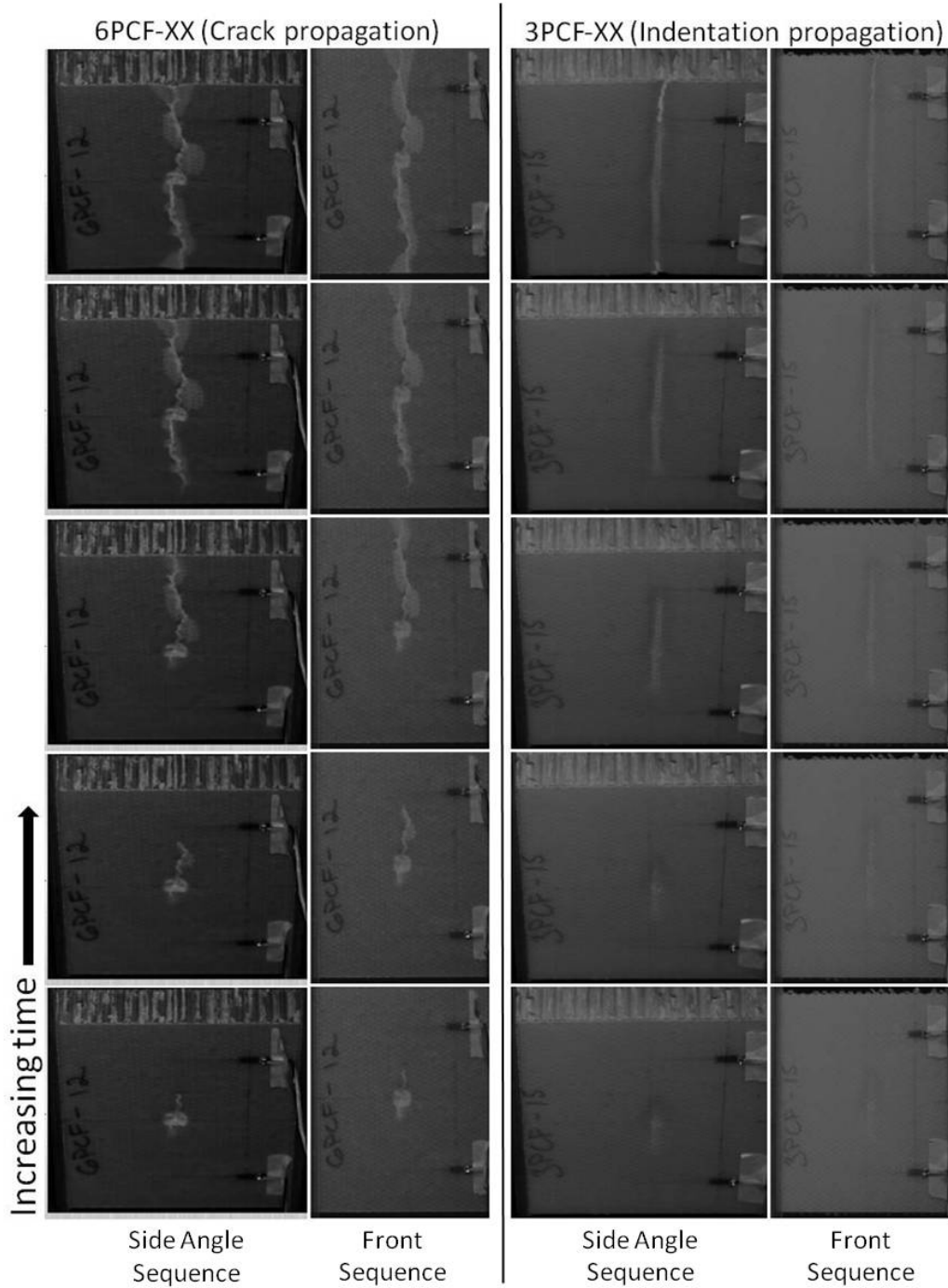


Fig. 26 Images taken from high speed cameras during failure of 3PCF-XX (right) and 6PCF-XX (left) materials.

although it propagates to the right slightly before the left showing that there may be a difference in stress concentration on either side of the initial damage due to impact damage asymmetry. In real time, however, this was not noticeable for most test cases. Photos, taken at high speed, of coupon

3PCF-15 show indentation propagation failure. With the aid of the side mounted camera, the high speed camera footage clearly shows the out-of-plane deflection in the locally buckled region. Also, in both cases the failed facesheet's inability to transfer load causes the entire coupon to buckle globally. Although the global out-of-plane displacement at the middle point of the coupon is small it can be seen in the side images taken from the high speed cameras. In the actual video, this feature is easier to see, as the coupon can be seen to actually move.

Nominal failure stress was calculated from the measured resultant force divided by the nominal cross sectional facesheet area of each coupon and is shown in Fig. 27. Average measured far-field strain at coupon failure from the four strain gages on each panel was also reported for each coupon, which is shown in Fig. 28. Additional detailed CAI test results can be found for these tests in Ref. [3].

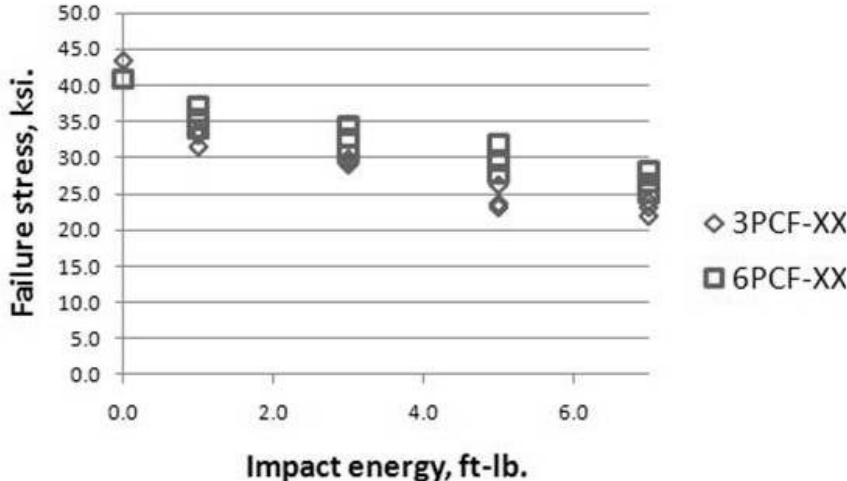


Fig. 27 CAI test results: failure stress vs. impact energy.

The failure strength of both 3PCF-XX and 6PCF-XX series coupons is shown to drop dramatically even for lightly impact-damaged specimens. The reduction in coupon strength of roughly 10 ksi from undamaged specimens to damaged specimens impacted at 1.0 ft-lb. energy levels was higher than any subsequent drop, even in the most damaged sandwich panels. The drop of failure strength is shown to decrease in severity with further increasing levels of damage. Tests of 3PCF-XX series panels with a given damage level were more repeatable in terms of their failure level than tests at 6PCF-XX series panels. It is also important to note that failure of 6PCF-XX panels impacted at a

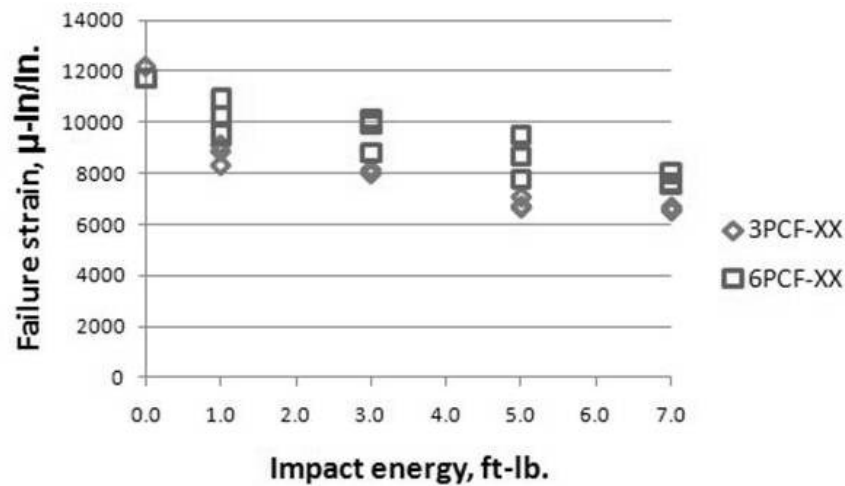


Fig. 28 CAI test results: failure strain vs. impact energy.

given energy level occurred at higher stress and strain levels than 3PCF-XX panels. This suggests that the higher density honeycomb core found in 6PCF-XX panels contributes to the increased CAI strength. It was shown previously that the residual dent increases dramatically in size for the 3PCF-XX specimens, while the dent does not increase in size noticeably for the 6PCF-XX specimens. This is likely due to the higher strength and stiffness of the higher density core in response to out-of-plane compressive loads. This loading occurs when the already indented facesheets press inwards at the edges of the initial dent due to the applied compressive load to the panel. The higher out-of-plane stiffness precludes the indentation propagation failure mode; instead, the panels fail due to crack propagation due to in-plane stress concentrations in the facesheet which cause material fiber and matrix failure.

C. Further CAI Results: Digital Image Correlation

A DIC system was used for full field displacement and surface mapping of a select group of CAI test coupons for the 3PCF-XX and 6PCF-XX series materials. The DIC system provided important information about the shape and deformation of impact damage in each test coupon surveyed. It also helped to validate observations on the differences between the two observed CAI failure modes, indentation propagation and crack propagation, which were made through time lapse imagery from video footage. The DIC system allows observations about damage growth to be quantified. An

example of a 3D DIC representation is shown in Fig. 29. A 3PCF-XX coupon is shown here, after failure.

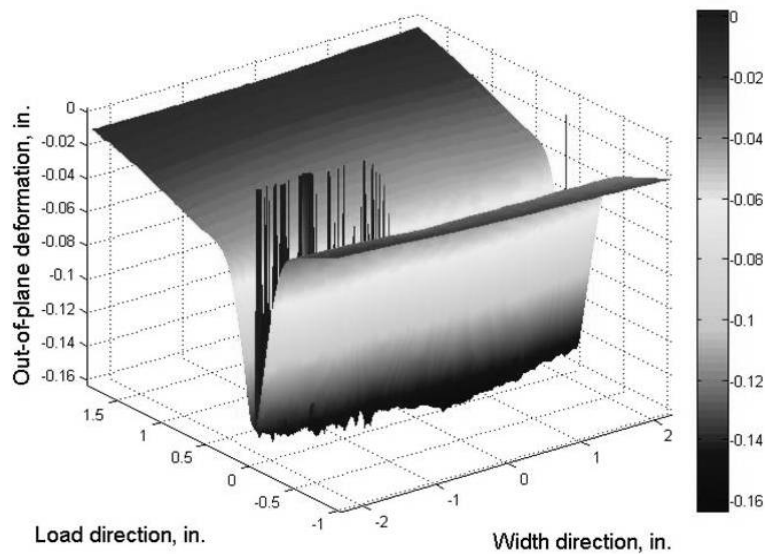


Fig. 29 Example 3D representation of the indentation propagation failure mode for a 3PCF-XX series CAI test coupon.

The main benefit of the DIC system to the present research was the ability to quantify the change in size of the out-of-plane impact damage in the damaged facesheet of the sandwich panel test coupon during subsequent compressive loading. Four test coupons from both the 3PCF-XX and the 6PCF-XX series materials were selected for instrumentation using the DIC system. For the 3PCF-XX series tests, coupons 3PCF-05, 3PCF-03, 3PCF-10, and 3PCF-09 were selected to represent the four impact energies used for impacting 3PCF-XX series CAI test coupons, which were 1.0, 3.0, 5.0, and 7.0 ft-lb., for the four coupons, respectively. For the selection of results presented, the dent on each test coupon was measured in the direction of the coupon width (X-direction), in the coupon load direction (Y-direction), as well as its depth (out-of-plane or Z-direction). These measurements were made at 0%, 50%, 75%, 90% and 100% (just prior to failure) of the test coupon's failure load, and a spline fit curve was applied to the data points.

The results for the coupon width direction measurements are shown in Fig. 30; the load direction measurements are shown in Fig. 31; the dent depth measurements are shown in Fig. 32 for the 3PCF-XX series test coupons. The size of the impact damage in each coupon does not appreciably

increase in size prior to 50% of the eventual test coupon failure load. Subsequently, the size in the coupon width direction can increase in a stable fashion to as much as one third of the overall coupon width (5.5 in.). The impact damage size remains constant in the load direction. The depth of the impact damage also increased during testing for each of the coupons studied with the DIC system.

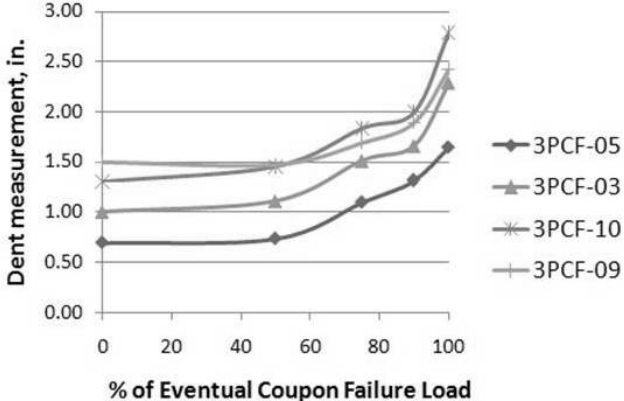


Fig. 30 Results from DIC Measurements: dent growth in coupon width direction for 3PCF-XX test coupons.

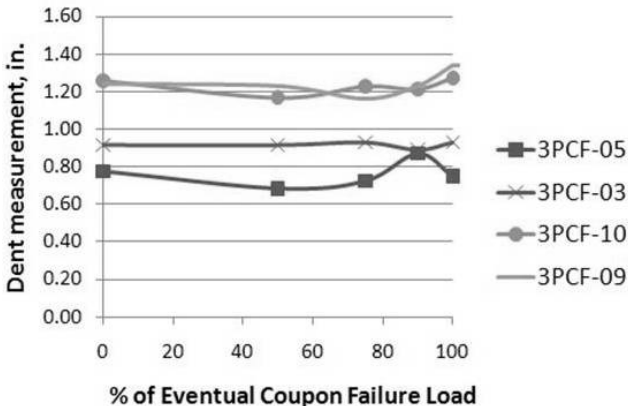


Fig. 31 Results from DIC Measurements: dent growth in coupon load direction for 3PCF-XX test coupons.

For the 6PCF-XX series material, test coupons 6PCF-10, 6PCF-09, 6PCF-06, and 6PCF-11 were chosen for DIC system observation during compression loading. These panels were impacted at energy levels of 1.0, 3.0, 5.0, and 7.0 ft-lbs., respectively. The impact damage growth was again measured for size in the coupon width and load directions, as well as maximum depth. The results for the width direction measurement are shown in Fig. 33; the load direction results are shown in

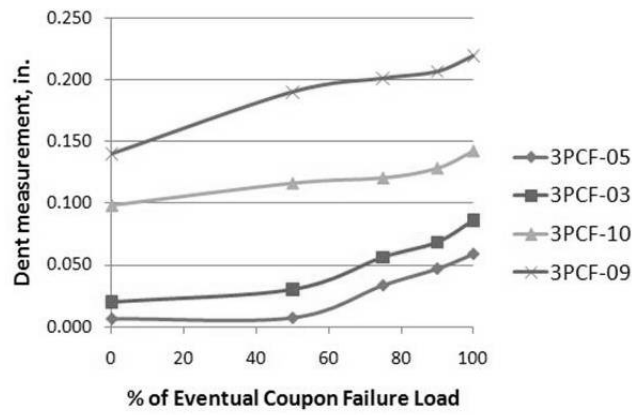


Fig. 32 Results from DIC measurements: dent depth increase for 3PCF-XX test coupons.

Fig. 34, and the dent depth measurements are shown in Fig. 35. The dent growth measured for the 6PCF-XX test coupons was not nearly as marked as for 3PCF-XX and PXX series coupons. Generally, most of the dent growth for 6PCF-XX test coupons occurred very near to failure, at greater than 90% of the eventual failure load. Additionally, the stable growth amount was much smaller than 3PCF-XX coupons, when compared in terms of total growth, as well as in terms of percentage of test coupon size. Presumably, the reduced amount of damage growth in 6PCF-XX series coupons is due to the high strength and stiffness of the higher density core material. Since, any dent growth must be precipitated by crushing of the honeycomb core underneath the facesheet indentation, a higher stiffness and strength of the core should lead to less growth, in general.

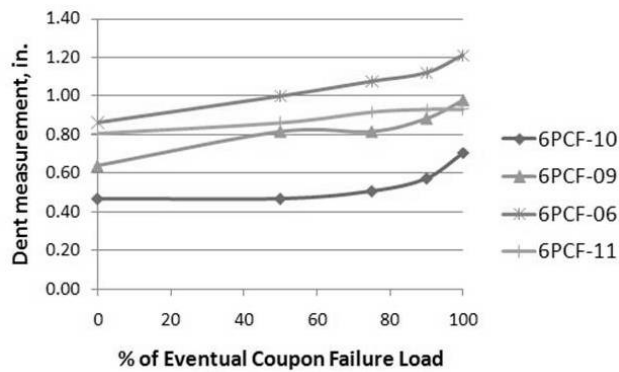


Fig. 33 Results from DIC measurements: dent growth in coupon width direction for 6PCF-XX test coupons.

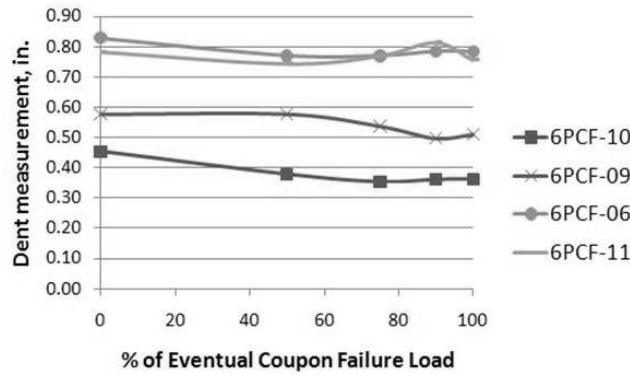


Fig. 34 Results from DIC measurements: dent growth in coupon load direction for 6PCF-XX test coupons.

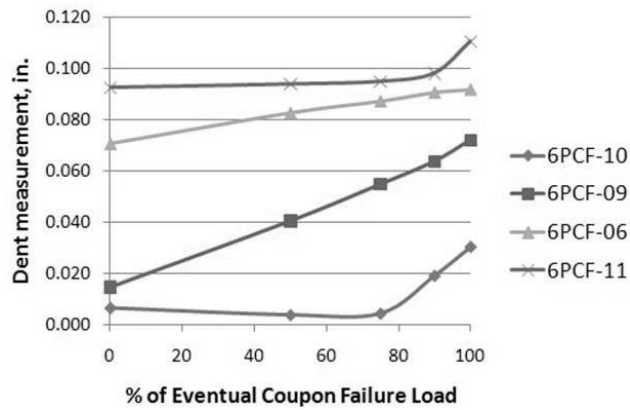


Fig. 35 Results from DIC measurements: dent depth increase for 6PCF-XX test coupons.

V. Conclusions

Composite structures are increasingly being considered as lightweight alternatives in the design of tomorrow's aerospace vehicles, from small private propeller-driven planes, to the newest commercial jetliners, and the next generation of heavy lift vehicles for future space exploration. They are already used extensively in modern commercial satellites. Currently, some of the major design challenges in composites pertain to the understanding of damage formation and response of a composite structure with damage present. One aspect of the latter challenge is the understanding of composite sandwich structure response to compression after low velocity impact. This has been the subject of the present research, which has included both experimental testing and finite element analysis (FEA). Part 1 of the research, which has focused solely on the experimental results of the current research, has been the focus of this paper.

The experimental testing techniques were introduced and the testing results were summarized for two Nomex honeycomb core sandwich panel constructions with thin woven fiberglass facesheets. Damage formation was studied, as well as the CAI response. In addition, unique instrumentation and observation techniques were used to gain a detailed understanding of these tests. The two material systems considered in the present document were identical to each other, except for one important difference. The density of the honeycomb core, 3 lb/ft³ in one material (3PCF-XX), and 6 lb/ft³ in the other (6PCF-XX), was used to assess the core density's effect on damage formation and CAI response.

Low velocity impact testing using a drop tower was conducted to study damage formation in each of the materials. Impact force vs. time data was collected for each impact test coupon. Force was found to increase with impact energy until facesheet fracture occurred. The maximum force recorded for higher energy impacts did not increase, although the length of the impact did increase. The types of damage found for drop impact was similar to static indentation. The depth and diameter of the impact damage dent was found to increase to a maximum before leveling with increasing impact energy. On the other hand, the amount of matrix and fiber cracks did continue to increase with impact energy. The damage formation study was used to select the impact energy levels of interest which were then used in CAI tests.

Failure in the front, damaged facesheet of each material coupon was found to be the principal factor in global panel failure due to compressive loading. Panel failure was found to be indicated by a sudden, instantaneous drop in the force vs. displacement curve for each coupon. Failure strength for CAI specimen was compared to the compressive strength of an undamaged specimen. The reduction in residual strength of a material coupon was found to be most severe for lightly damaged coupons. Increasing levels of damage resulted in further reduction in residual strength, but the reduction between adjacent data points decreased in magnitude. New insight was gained into the CAI response and ultimate failure of test coupons using novel instrumentation techniques. High speed video photography captured images of failure. These images were not previously available in the literature.

Two CAI failure modes were found during the experimental investigation. In material systems

with 3 lb/ft³ density honeycomb cores, an indentation propagation failure mode resulted which is essentially a local buckling of the facesheet due to the collapse of the honeycomb core beneath. A crack is present in the facesheet, but the propagation of the residual indentation transversely across the facesheet precedes the crack. In testing of the higher density, 6 lb/ft³ core materials, a second failure mode was found, which was termed crack propagation. A transverse fiber crack propagates across the facesheet, without any local facesheet buckling or core crush. Since the 3PCF-XX and 6PCF-XX series panels are identical except for the honeycomb density, the failure mode was found to be dependent on core density. Full field measurements using the DIC system and VIC-3D software also demonstrated the difference in the two failure modes. It was concluded that the higher density core also resulted in very little dent growth, prior to failure. The effect of core density on damage formation and CAI response in honeycomb core sandwich panels also highlighted the need for new analysis techniques. These analysis techniques will be the subject of Part 2 of the research.

Acknowledgments

This research was completed with the laboratory and financial resources of NASA Langley Research Center (LaRC), in Hampton, VA, through a partnership between NASA LaRC, the National Institute of Aerospace (NIA), and Virginia Tech.

References

- [1] Tomblin, J., Lacy, T., Smith, B., Hooper, S., Vizzini A., and Lee, S., "Review of Damage Tolerance for Composite Sandwich Airframe Structures," *FAA Technical Report*, DOT/FAA/AR-99/49, U.S. Dep. of Transportation, Federal Aviation Administration, Office of Aviation Research, Washington, DC, August 1999.
- [2] "Composite Aircraft Structure," *FAA Advisory Circular*, AC 20-107B, CHG 1, U.S. Dep. of Transportation, Federal Aviation Administration, Washington, DC, August 2010.
- [3] McQuigg, T., "Compression After Impact Experiments and Analysis on Honeycomb Core Sandwich Panels with Thin Facesheets," Ph.D. Dissertation, Virginia Polytechnic Institute and State University, Blacksburg, VA, May 27, 2011.
- [4] Raju, K., Smith, B., Tomblin, J., Liew, K., and Guarddon, J., "Impact Damage Resistance and Tolerance of Honeycomb Core Sandwich Panels," *Journal of Composite Materials*, Vol. 42, No. 4, 2008, pp.

- [5] Singh, A., Davidson, B., Eisenberg, D., Czabaj, M., and Zehnder, A., "Barely Visible Impact Damage Evaluation of Composite Sandwich Structures," *51st AIAA/ASME/ASCE/AHS/ASC Structures, Structural Dynamics, and Materials Conference*, Orlando, FL, April 2010.
- [6] Cantwell, W., and Morton, J., "The Significance of Damage and Defects and Their Detection in Composite Materials: A Review," *The Journal of Strain Analysis for Engineering Design*, Vol. 27, No. 1, 1992, pp. 29 - 42.
- [7] Tomblin, J., Raju K., Liew, J., and Smith, B., "Impact Damage Characterization and Damage Tolerance of Composite Sandwich Airframe Structures," *FAA Technical Report*, DOT/FAA/AR-00/44, U.S. Dep. of Transportation, Federal Aviation Administration, Office of Aviation Research, Washington, DC, January 2001.
- [8] Rhodes, M., "Low Velocity Impact on Composite Sandwich Structures," *2nd Air Force Conference on Fibrous Composites in Flight Vehicle Design*, May 1974.
- [9] Rhodes, M. "Impact Fracture of Composite Sandwich Structures," *16th AIAA/ASME/SAE Structures, Structural Dynamics, and Materials Conference*, 1975.
- [10] Tsang, P.H., and Lagace, P., "Failure Mechanisms of Impact-Damaged Sandwich Panels Under Compression," *35th AIAA/ASME/ASCE/AHS/ASC Structures, Structural Dynamics and Materials Conference*, 1994.
- [11] "ACG MTM45-1 6781 S-2 glass 35% RC," *Qualification Material Statistical Analysis Report*, CAM-RP-2009-001, National Center for Advanced Materials Performance, NASA, National Institute for Aviation Research, Wichita State University, KS, February 2010.
- [12] "HexWeb Honeycomb Attributes and Properties," HexCel Composites, Inc., 1999, URL: http://www.hexcel.com/Resources/DataSheets/Brochure-Data-Sheets/Honeycomb_Attributes_and_Properties.pdf [cited June 21, 2011].
- [13] "Standard Test Method for Compressive Residual Strength Properties of Damaged Polymer Matrix Composite Plates," *ASTM Test Standard*, D 7137/D 7137M 07, December 2007.
- [14] "Standard Test Method for Edgewise Compressive Strength of Sandwich Constructions," *ASTM Test Standard*, C 364/C 364M 07, April 2007.
- [15] Phantom High Speed Cameras, Vision Research, Inc., URL: www.visionresearch.com.
- [16] VIC-3D 2010, Correlated Solutions, Inc., URL: www.correlatedsolutions.com.
- [17] Sutton, M., Orteu, J., and Schreier, H., *Image Correlation for Shape, Motion, and Deformation Measurements: Basic Concepts, Theory, and Applications*, Springer. New York, NY, 2006.